ACS OMEGA

Open Access

http://pubs.acs.org/journal/acsodf

Article

Numerical Simulation and Parameter Optimization for Water-to-CO_2 Flooding in a Strongly Water-Sensitive Reservoir

Published as part of ACS Omega virtual special issue "CO2 Geostorage".

Xu Deng, Meilong Fu,* Jie Li, Jiani Hu, Guojun Li, and Fankun Meng

Cite This: *ACS Omega* 2024, 9, 9655−9665

Read Online

ACCESS | Metrics & More | Article Recommendations

ABSTRACT: Carbon dioxide flooding can accelerate the development of low-permeability reservoirs of the Kexia group in the K region of the T oil field, thus resolving the issue of inadequate water drive effects. This study was focused on the well group 80513 in the K region, and based on the reservoir and fluid parameters, a simulation model of water-sensitive post-CO_2 flooding was constructed to refine the gas injection strategy gradually. The injection rate of the continuous gas injection stage was preferred based on the degree of recovery. Multiindicator and multifactor injection and extraction schemes were established to optimize and analyze the key controlling factors, including the gas injection rate, gas injection period, gas-to-water ratio, and bottom-hole flow pressure, in the carbon dioxide gas-to-water alternation process. Recovery efficiency, oil exchange rate, formation pressure, and carbon dioxide storage rate were used as indicators. After 5 years of continuous CO_2 flooding, the results indicated that switching to CO_2 gas−water alternating flooding was more appropriate for the target block's environment. The best development plan was achieved when the gas injection rates were 1.0 and 1.25 × 10^4 $m^3 \cdot d^{-1}$ for continuous gas injection and CO_2 gas−water alternating flooding, respectively, with a gas−water ratio of 1:1, a gas injection cycle of 90 days, and a bottom-hole flow pressure of 25 MPa in the production wells. A comparison between the results revealed that the formation pressure and oil recovery efficiency of this well group significantly increased upon CO_2 flooding, and the parameter optimization results were well suited for controlling the gas flurry, offering a versatile model for future development of the block.

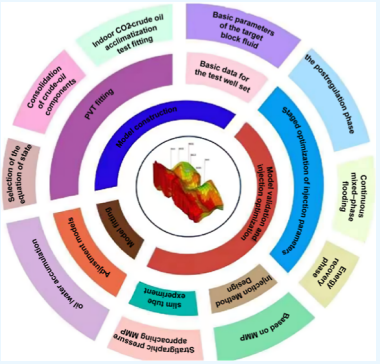

1. INTRODUCTION

The most practical option for energy replacement in China is unconventional oil and gas resources, which are exemplified by tight oil reservoirs with poor permeability.[1,2] Developing a geological engineering integration technology system appropriate for China's land-phase tight oil reservoirs, in accordance with various types of oil reservoirs, is imperative in view of the ongoing advancements in oil and gas exploration and development. Such a system will aid in boosting production capacity, reducing costs, and realizing the scale of increasing reserves and building production of complex oil and gas reservoirs, such as tight oil.[3] The K-zone of the T oil field is a typical strongly water-sensitive, low-permeability reservoir with poor physical characteristics. At the end of 2016, 69 oil and water wells (48 oil wells and 38 open wells) with an average daily production of 0.7 t of oil, a water cut of 68.8%, cumulative production of 16.83 × 10^4 t of oil, an 8.4% recovery efficiency, and a 0.32% oil recovery rate were present in the block. The block has been under development since the 1990s; since then, the development of 20 open and 20 water injection wells along with a monthly injection/production ratio of 0.63, a total water injection of 37.41 × 10^4 m^3, and a 52% oil saturation have been realized. To achieve cost reduction and high efficiencies, the driving mechanism needs to be modified because, until 2016, a major area of the study region had inadequate water injection as well as low formation energy and recovery efficiency due to low permeability and formation sensitivity.

The carbon industry, a globally recognized sunrise industry, not only involves the traditional energy, construction, and financial sector but also integrates environmental protection and green development of the Earth.[4] In the pursuit of low-carbon energy transition, the proposal of carbon dioxide capture, utilization, and storage (CCUS) has strengthened research on carbon resource utilization technologies and promoted their application. Therefore, since the "11th Five-Year Plan" period, under the national strategy, a number of key national science and technology programs, such as the Natural

Received: December 5, 2023
Revised: January 23, 2024
Accepted: January 25, 2024
Published: February 12, 2024

Science Foundation and 973 Program, have stepped up support for research and development on the CCUS technology system. Through strengthening basic theoretical research, overcoming technical difficulties, project integration, and demonstration, each technical aspect of carbon dioxide capture, transportation, utilization, and storage has been rapidly developed, and a series of successful results have been achieved.[5,6] Thus, far, the first-generation CCUS technology has been built, with almost perfect theoretical support and supporting conditions, and has been successfully applied to unconventional oil reservoirs numerous times.[7−9] CO_2 flooding is widely used in China and abroad as a high-efficiency recovery technology, which can expand the microscopic wave area and improve the efficiency of oil drive by expanding the volume of crude oil and reducing the viscosity and interfacial tension of crude oil. Several in-house experiments, such as constant composition expansion experiments, multistage degassing experiments, and field practices, have demonstrated that CO_2 flooding can help enhance the recovery of low-permeability nonhomogeneous reservoirs.[10−15] Currently, CO_2 flooding is mostly applied to medium-low permeability reservoirs, on the one hand, water flooding in this kind of reservoir can achieve good results, and the reference to ultralow permeability reservoirs is limited; on the other hand, China has not yet formed a stable industrial structure of CO_2 gas source, and the cost is high, which restricts the large-scale application of CO_2 flooding technology.[16,17]

Numerical simulations yield the distribution of different phases after CO_2 injection and can optimize the injection parameters. Xia et al. numerically simulated the carbon dioxide flooding for a low-permeability reservoir with formation deficit and difficulty in water drive development. They optimized the well network spacing, well spacing, and gas injection methods to derive a reasonable injection and extraction scheme.[18] Song et al. carried out numerical simulation-based parameter optimization of CO_2 flooding to assess the issues hampering water drive development in nonhomogeneous, low-permeability reservoirs. Although the preferred scheme is reasonable, the level values set for each factor were less, resulting in fewer preferred injection and recovery schemes.[19] Shang et al. numerically simulated CO_2 flooding in a low-permeability reservoir with poor physical properties and difficult water drive utilization. They reasonably optimized the injection and recovery parameters, but the analytical method used to analyze the results of injection and recovery did not consider the differences among the various indices.[20] Wang et al. established a numerical simulation model for the flooding of CO_2 in a nonhomogeneous reservoir. This model evaluated the potential of EOR as well as assessed the feasibility of CO_2 flooding and storage, but only based on a single-factor preference, and only a small number of indicators were considered.[21] Bai carried out indoor experiments and numerical simulations of CO_2 flooding based on the physical characteristics of a strongly water-sensitive reservoir with difficult water-drive development. The recovery rate predicted by this simulation model was 17.3% higher than that of the water drive, and the optimized injection and extraction scheme was highly feasible.[22] Lu et al. established a numerical simulation model of CO_2 flooding and obtained an optimal carbon dioxide throughput development scheme for a strongly water-sensitive thick oil reservoir with an insufficient formation energy and poorly developed water drive.[23] Zhuang et al. numerically simulated the CO_2 flooding for a low-permeability reservoir and effectively solved the problem of poor development effect of water injection in the reservoir by gas injection; the simulated recovery efficiency of oil production was 60%, which is a high value.[24] Overall, to date, extensive numerical simulation-based analyses of CO_2 flooding in low-permeability, nonhomogeneous reservoirs have been performed. However, studies on the numerical simulation of CO_2 flooding with strong water sensitivity are scarce.

A reasonable injection and recovery parameter design is crucial for oil field exploitation. To mitigate the poor water drive effect in low-permeability reservoirs of the K lower group in the K area of the T oil field, we propose utilization of CO_2 flooding to improve the development effect. The well group 80513 in the target block was studied as an example, and a numerical simulation model of carbon dioxide drive water sensitivity was established based on physical characteristics. The gas injection program was designed and optimized in phases over time, and finally, the recovery rate of this well group was used to generate a reference idea for the development of its location block.

2. CARBON DIOXIDE FLOODING MODELING

2.1. Basic Data for the Test Well Set. The reservoir of the target block of the T oil field is located on the northwestern margin of the Junggar Basin and in the lower part of the Nanbaijiantan and Kewu faults, while the target block is located in the southeast extended area (as shown in Figure 1). The block is located in the Lower Kehl Formation,

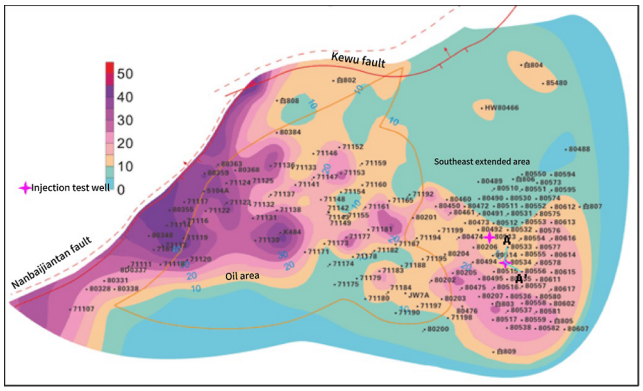

Figure 1. Contour map of the oil layer's thickness in the reservoir in the target block.

which is an S_7 sand formation, with five sand types that can be subdivided into S_7^1, S_7^2, S_7^3, S_7^4, and S_7^5. The main layers S_7^5 and S_7^4 are dominated by subphase deposition in the deltaic plain with high stability and continuous sand body development, showing thin, multiple, and scattered characteristics in the longitudinal direction. According to the logging interpretation after the water drive, the porosity distribution range of the oil-bearing layers S_7^5−S_7^2 is 6.92−13.57%, and the permeability is $(2.46-23.72) \times 10^{-3}$ μm^2. Permeability coefficient of variation greater than 2, more inhomogeneous. The pore penetration characteristics of the block are characterized by better conditions in the central part and worse conditions in the upper and lower parts of the block (Table 1). The effective thickness of the zone, oil saturation, viscosity of the formed crude oil, and recovery efficiency are 18.9 m, 52%, 2.9 mPa·s, and 10.67%, respectively. The reservoir is dominated by conglomerates, with clay minerals

https://doi.org/10.1021/acsomega.3c09718
ACS Omega 2024, 9, 9655−9665

Table 1. Porosity and Permeability of the Logged Wells in the Study Area

	porosity/%			permeability/10^{-3} μm^2		
layer	maximum	minimum	average	Maximum	minimum	average
S_7^2	11.9	6.9	10	18.6	1.5	5.3
S_7^3	13.6	9.5	11.5	23.7	1.8	7.3
S_7^4	12.8	10.1	11.2	15.1	4.0	6.9
S_7^5	11.9	9.0	10.1	11.4	2.4	4.9

dominated by Illite/montmorillonite (average 34.2%) and kaolinite (average 30.4%), followed by small amounts of chlorite (average 18.3%) and Illite (average 17.1%).[25] The determined contents of various clay minerals in the target reservoir indicate that the reservoir is potentially water-, quick-, and salt-sensitive. Results of water sensitivity evaluation experiments reveal that the average water sensitivity index of the target reservoir is 0.60−0.83, which indicates moderately high water sensitivity, and the quick sensitivity index is in the range of 0.50−0.88.

2.2. Pressure−Volume−Temperature Matching. Because the CO_2 flooding process involves mass transfer between phases, numerical simulations of CO_2 flooding are based on component models, and to identify a suitable equation of state, a pressure−volume−temperature (*PVT*) fitting model is required. *PVT* fitting is conducted based on the phase simulation module of the Computer Modeling Group simulation software, which fits the parameters of the equation of state to experimental data of indoor CO_2−crude oil acclimatization. First, the equation of state is determined, followed by the fitting analysis; different equations of state exhibit different strengths and weaknesses as well as different computational accuracies for critical points. Typically, three-parameter state equations, i.e., Soave−Redlich−Kwong (SRK) and Peng−Robinson (PR) equations, are used in the component models. In the SRK equation, which was proposed by Soave in 1972 as an improvement of the RK equation of state, the $a/T_{0.5}$ term in the RK equation is replaced by a temperature function $\alpha(T)$ and corrected values of coefficients a and b.[26] The SRK equation is mostly applied to gas−liquid equilibrium calculations related to nonpolar molecules. The PR equation, proposed by Peng et al. in 1976, is based on the RK and SRK models and is characterized by further modified parameters.[27] The PR equation is more suitable for gas−liquid equilibrium calculations of systems with more polar components, such as CO_2, H_2S, and so on, as well as yields the properties of heavy components with high accuracy. The crude oil in the target block contains a high fraction of heavy components, and the three-parameter PR equation of state with volume correction coefficients is finally adopted to fit the equation of state using van der Waals' one-parameter mixing rule.[28] During the fitting of the CO_2−crude oil experimental data with the built-in PR equation of state, the final error is controlled within reasonable limits.

2.3. Consolidation of Crude-Oil Components. Indoor experiments performed to analyze the composition of crude oil in the target block show that the sum of the heavy and light fractions is greater than 30, and parallel calculation, which requires merging of the fractions, is challenging. Considering the limitations of computing time and equipment, the WINPROP module is utilized to "merge and process" the crude-oil fractions into a number of proposed fractions. According to the *K*-value equilibrium theory, the number of proposed components is obtained by dividing the light component by the heavy component, and then multiple merging schemes are obtained by dividing the light component by the heavy component. Finally, the best merging scheme is selected based on the bubble and dew point lines of each scheme. The final crude-oil fractions are divided into seven proposed fractions, i.e., CO_2, N_2/CH_4, C_2-nC_4, iC_5-C_7, C_8-C_{13}, $C_{14}-C_{24}$, and $C_{25}-C_{36}$. The adjusted parameters of the equation of state are compatible with the data of indoor constant composition expansion experiments, gas injection expansion experiments, multistage degassing experiments, and other crude oil−CO_2 adaptability experiments and yield good results with errors controlled within allowable limits. The fluid model obtained by combining the components and adjusting the equation of state is suitable for the studied block and can be applied to evaluate CO_2 flooding in the target block.

2.4. Model Construction. The fluid model is obtained through *PVT* fitting, combined with physical parameters and introduction of water-sensitive change rules based on GEM (component simulator), and establishes a numerical simulation model of CO_2 flooding, wherein the target well group is located in the block fluid, whose basic parameters are shown in Table 2.

Table 2. Basic Parameters of the Target Block Fluid

category	parameter	category	parameter
layer	S_7^{5-2}, S_7^{5-1}, S_7^{4-2}, S_7^{4-1}, and S_7^{4-3}	reservoir temperature/°C	65.4
geological reserves/10^4 t	192.7	saturation pressure/MPa	20.41
midpoint of pay zone/m	2258	viscosity of formation crude oil/(MPa·s)	2.9
effective thickness of oil layer/m	19.6	original formation pressure/MPa	31.60
porosity/%	10.14	oil saturation/%	50. 5
average permeability/$\times$ 10−3 μm^2	8.05	oil volume factor	1.301
density of degassed crude oil/(g/cm^3)	0.7581	solution gas−oil ratio/(m^3·t^{-1})	102

There are seven injection and extraction wells in the target well group, and an antiseven-point method well network with good well conditions is observed. Five small layers, such as S_7^{5-2}, S_7^{5-1}, S_7^{4-2}, S_7^{4-1}, and S_7^{4-3}, are selected for modeling in the vertical direction, and in the planar grid setup, the *X*- and *Y*-direction steps are 15 m, while the *Z*-direction grid step is 4 m. The model is constructed in the vertical direction. The on/off switching of the gas/water injection wells and the amount of injection are controlled by establishing a cyclic-controlled well group. CO_2 injection well constraints: surface liquid rate (STG) 1.0e^{6}m^3/day (MAX), bottom hole pressure (BHP) 40,000 KPa (MAX); water injection well constraints: surface water rate (STW) 800 m^3/day (MAX), BHP 40,000 KPa (MAX). Production well constraints: surface liquid rate (STL) 200 m^3/day, BHP 7000 kPa. The oil production wells are produced at a constant pressure, and the flow pressure at the bottom of the injection wells is set to be less than the formation rupture pressure. Based on the prediction results of the recovery efficiency under the sealing conditions with different gas−oil ratios, the recovery efficiency of a single well is the highest when the gas−oil ratio is 1600 m^3/t, and the model shuts down the extraction wells as the gas−oil ratio of a single well exceeds 1600 m^3/t. Oil and gas and oil−water

https://doi.org/10.1021/acsomega.3c09718
ACS Omega 2024, 9, 9655−9665

permeability data are obtained from the experiments, and a CO_2 flooding numerical simulation model is established for the target well group by combining the fluid model, basic physical parameters of the reservoir, well network data, and production dynamics data. The initial gas injection rate is 1.50×10^4 $m^3 \cdot d^{-1}$. To reflect the impact of strong water sensitivity on reservoir development, the effect of water sensitivity is incorporated into the model by setting up wells between injection and extraction wells that do not participate in the injection and by assigning permeability values obtained from logging to the wells. Finally, the actual permeability of the wells after water injection through automatic interpolation between wells is obtained. Studies have shown that there is a power relationship between water sensitivity damage rate and permeability.[29] The calculation of the actual permeability relies on the average water sensitivity index, which is 0.7. The actual permeability is equal to the pore volume (PV) multiple of the injected water multiplied by the water sensitivity index multiplied by the logging permeability. The well group's J direction permeability and porosity model is illustrated in Figures 2 and 3.

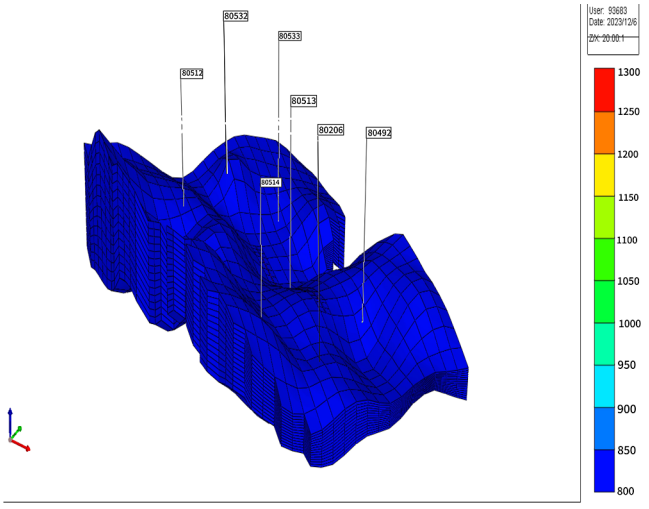

Figure 2. Schematic of the 3D model of J direction permeability in well group 80513.

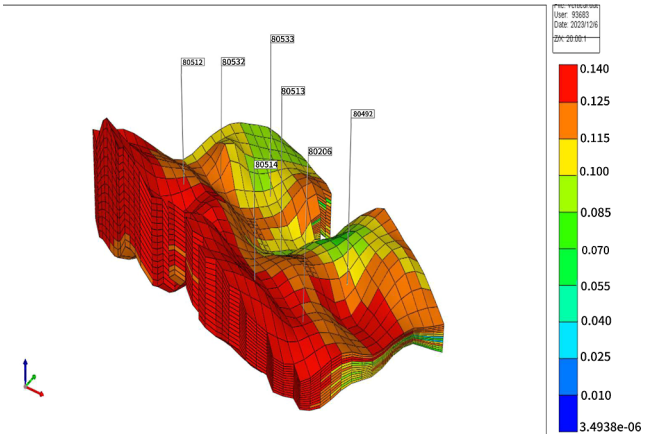

Figure 3. Schematic of the 3D model of porosity in well group 80513.

2.5. Model Fitting. The calculated results of the model reveal that in the pretest injection, the well group's average daily output is 13t/d, with a water cut of almost 60%. Oil recovery surpasses water drive, and the water cut remains almost the same. However, after 3 years of injection, the water cut decreased by about 7 points. The results of the numerical simulation are fitted to the field development data using cumulative oil production and cumulative water content as fitting indices, and a fitting error of less than 5% is obtained, which satisfies the simulation accuracy criteria (Figure 4).[30]

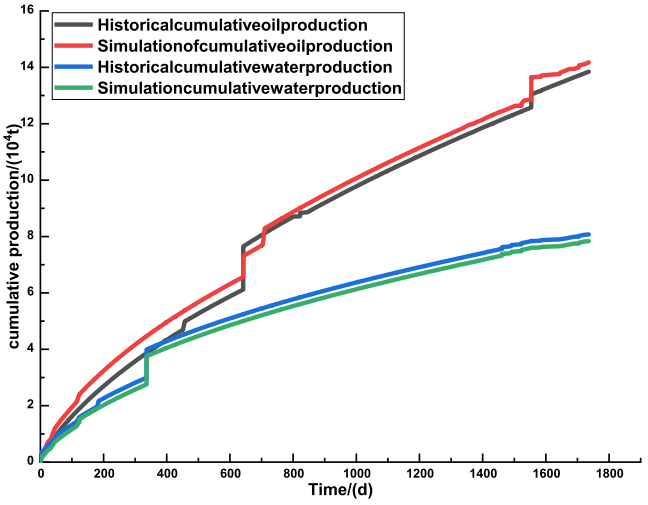

Figure 4. Target well group cumulative production history fit.

These fitting results indicate that the numerical simulation model reproduces well the characteristics of the target well group, thus confirming the validity of the proposed model and guaranteeing good agreement between the model's output and the reservoir's real development scenario.

3. MODEL VALIDATION AND INJECTION OPTIMIZATION

3.1. Method for Carbon Dioxide Drive Parameter Optimization. Field data indicate that the formation pressure in the production wells of this well group is ~17.5 MPa, which may be lower than the minimum miscibility pressure of CO_2 flooding. Therefore, restoring the formation pressure is necessary. To realize rational development, optimization of the CO_2 injection parameters for well group 80513 is divided into three parts based on time sequence and the characteristics of the reservoir in which the target well group is located: energy recovery phase, continuous gas injection phase, and regulation and optimization phase. The gas injection rate is optimized based on the field data of the energy recovery phase, whereas the continuous gas injection and regulation optimization stage is based on the established model for parameter optimization, which mainly includes key parameters such as gas injection rate, gas injection period, gas−water ratio, and bottom-hole flow pressure. Because of the risk of CO_2 flooding gas channeling, in which the wells are shut down because of long-term continuous gas injection, the choice of injection method in the regulation and optimization stage is primarily based on blocking the gas channeling and improving the flow ratio to slow the CO_2 flooding gas channeling.

3.2. Determination of Minimum Mixing Pressure. The minimum miscibility pressure for carbon dioxide−oil repulsion in the target area is determined according to SY/T 6573-2016 "Experimental determination of minimum miscibility pres-

https://doi.org/10.1021/acsomega.3c09718
ACS Omega 2024, 9, 9655−9665

sure—Fine tube method".[31] A crude-oil sample collected from the K lower group formation in the K area was selected for the experiment, and the recovery efficiency at formation pressures of 21.2, 22.4, 23.2, 25.8, 27.8, and 31.8 MPa was simulated via thin-tube experiments with a preset injection volume of 1.2 times the PV (Figure 5). Figure 5 shows that the minimum

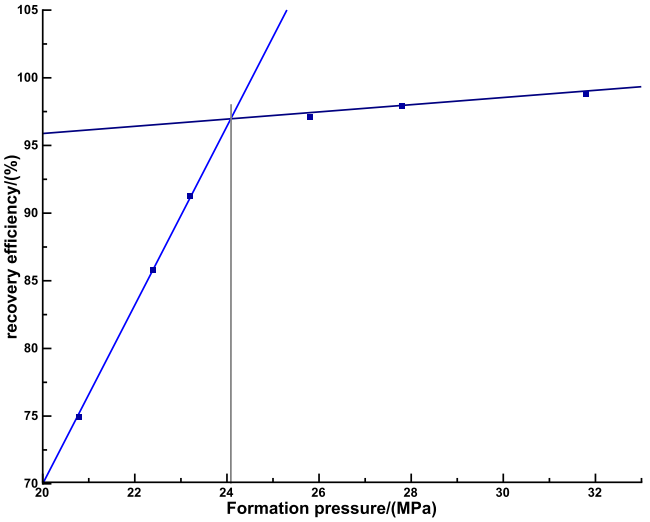

Figure 5. Calculation results of minimum miscible pressure in a slim tube experiment.

miscibility pressure is 24.1 MPa, and the formation pressure of the production well is 18 MPa, which is lower than the minimum miscibility pressure of carbon dioxide, and we first need to restore the formation pressure.

3.3. Energy Recovery Phase. Based on the minimum mixed-phase pressure, different stages of the injection scheme are obtained, and the CO_2 injection rate is now preferred for the first stage of energy recovery, based on the field trial injection data. The oil reservoir pressure is related to the flow pressure, which determines the oil pressure. Evidently, the oil pressure reflects the oil reservoir's pressure to a certain extent. The limited injection pressure is less than 20 MPa, and the site's designed gas injection rates are (1.0, 2.0, 2.5, and 3.0) × 10^4 $m^3 \cdot d^{-1}$. Figure 6 indicates that in the water injection stage, when the oil pressure is ∼20 MPa, the daily water injection rate is 12−20 $m^3 \cdot d^{-1}$; in the gas injection stage, when the daily gas injection rate is (2.5−3.0) × 10^4 $m^3 \cdot d^{-1}$, the oil pressure is ∼20 MPa, and the carbon dioxide injection capacity is ∼3.7 times of the water injection capacity. Thus, we finally reach the energy recovery stage with an injection rate between 2.5 × 10^4 and 3.0 × 10^4 $m^3 \cdot d^{-1}$.

3.4. Continuous Mixed-Phase Flooding. After the energy recovery phase, the formation pressure reaches MMP (minimum miscibility pressure), resulting in miscible carbon dioxide. Under the same conditions, the rate of gas injection in this stage is optimized based on the established numerical simulation model using the recovery efficiency from a single well in this stage as the indicator. Figure 7 shows that the highest recovery efficiency of 10.55% is achieved at a gas injection rate of 1.0 × 10^4 $m^{-3} \cdot d^{-1}$. This result demonstrates that the gas injection rate of the miscible carbon dioxide stage is 1.0 × 1 × 10^4 $m^3 \cdot d^{-1}$.

3.5. Parameter Optimization in the Postregulation Phase. Improvement of CO_2 flooding using water−gas alternating injection (WAG). This technology combines the advantages of water and gas injection, alternately injecting water and CO_2 plugs in sequence, and injected CO_2 can expand the macroscopic wave and volume of injected water and injected gas to improve the microscopic oil-driving efficiency. WAG can dramatically reduce the CO_2 fluidity after gas flooding, reduce the flow resistance of the oil phase, and increase the seepage resistance of the water phase, which makes it easier for crude oil to be driven out and plays a role in expanding the wave volume to improve the effect of oil drive. Hydrodynamic methods are effective in suppressing CO_2 flooding gas channeling in nonhomogeneous models, and the ability to suppress gas channeling is strongest when water and gas are injected alternately.[32,33] To design the injection

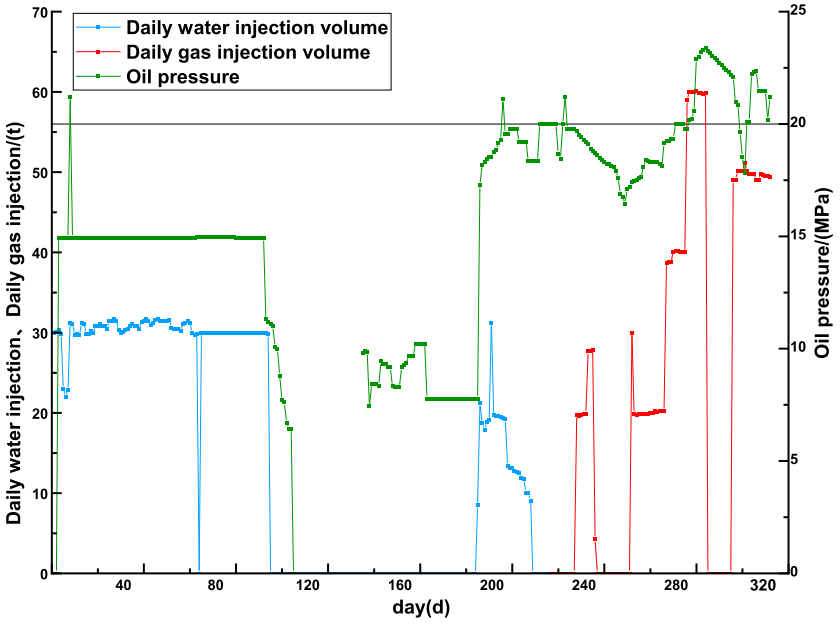

Figure 6. Gas and water injection curves for well group 80513.

https://doi.org/10.1021/acsomega.3c09718
ACS Omega 2024, 9, 9655−9665

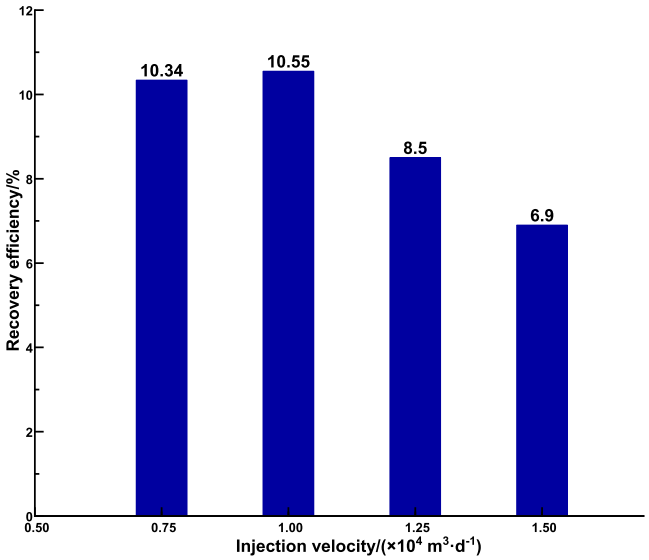

Figure 7. Recovery efficiencies with different gas injection rates.

scheme, a gas−water alternating injection method is used in the regulation and optimization phases, and several key injection parameters are utilized. After historical fitting, the model prediction results align well with the actual development within error tolerance. These results are then combined with the orthogonal design theory to establish a multifactor and multiindicator injection and extraction scheme to optimize the injection and extraction parameters of the CO_2 water and gas alternating part.[34,35] Several key factors affecting CO_2 gas−water alternation were selected as gas injection rate, gas injection period, gas−water ratio, and bottom-hole flow pressure, and four level values were selected for each factor respectively (see Table 3). The design and results of the

Table 3. Factors and Levels of Repulsion Influence

	level			
factor	1	2	3	4
gas injection rate/(×10^4 m^3·d^-1)	1.0	1.25	1.50	1.75
gas injection period/(mon)	2	3	4	5
gas−water ratio/(m^3·m^-3)	1:1	1:2	2:1	1:3
bottom-hole flowing pressure/MPa	10	15	20	25

multifactor and multiindicator injection and extraction program, using the recovery efficiency, oil exchange ratio, CO_2 storage rate, and formation pressure as development indicators, are shown in Table 4.

To assess the rationality of the replacement method, we consider several indicators because the different target items of each experimental program are not uniform. These different indicators are then used to set the scoring criteria for each program and select the most comprehensive implementation of the program. Recovery efficiency and oil exchange rate scores are proportional to the value of the index. The scoring criteria for the formation pressure and CO_2 storage rate are different from the other two indicators; for the formation range, the scores are obtained in the following sequence: 25−28 MPa > 29−34 MPa > 16−24 MPa > 34 MPa. The score gradually increases for storage rates: 35−40 < 40−45 < 45−50, and when the storage rate is greater than 50, a consistent score of 45−50 is obtained. Indicator criteria are based on the reference criteria of the study area established by Yu.[36] These results indicate that the highest overall score is obtained for experimental scheme no. 6 established in this simulation; that is, the gas injection rate is 1.25 × 10^4 $m^3·d^{-1}$, the gas-to-water ratio is 1:1, the gas injection cycle is 90 days, the bottom-hole flow pressure of the production well is 25 MPa, the recovery efficiency of the reservoir is 20.74%, the oil exchange rate is 21.33%, the formation pressure is 27.8 MPa, and the storage efficiency is 49.4%.

3.6. Adaptation of Optimization Results to Regulating Gas Channeling. For nonhomogeneous cores with permeability gradients ≤10, alternating gas−water drive can effectively control CO_2 flooding gas channeling, delay gas-channeling time, and increase the recovery efficiency by more than 17%.[37] In addition to basic physical parameters such as crude-oil viscosity and reservoir permeability, the injection rate and gas-to-water ratio also influence the CO_2 flooding gas channeling time. The optimization results of the control optimization stage should consider both the extraction and the prevention of CO_2 flooding gas channeling. Thus, next, we evaluate the adaptability of the optimized injection rate and gas−water ratio to regulating gas channeling. The gas-to-oil ratio rapidly increases in the gas scramble phase, and almost no crude-oil production is observed in this phase. The following is a comparative analysis of the change in gas-oil ratio, the timing of gas breakthrough and the sweep coefficient based on the injection speed and gas−water ratio of different horizontal values.

A comparative analysis of the gas-to-oil ratio changes, time of gas visualization, and wave coefficient based on different injection rates and gas-to-water ratios is performed. Figure 8 shows that when the gas injection rates are 1.5 × 10^4 and 1.75 × 10^4 $m^3·d^{-1}$, the amount of gas injected into the pore, whose volume is approximately 0.7 times the gas−oil ratio, changes with the changing gas−oil ratio. It first remains almost constant and then abruptly increases; at this point, the gas becomes visible. A gas volume equal to the PV of the gas channeling is a severe case. At injection rates of 1.0 × 10^4 and 1.25 × 10^4 $m^3·d^{-1}$, the gas starts appearing when a gas volume ∼0.8 times the PV is injected, and the gas channeling phenomenon is severe when the volume injected is 1.1 times the PV. A high injection rate results in a larger flow capacity and rapid movement of the leading edge. Further, the earlier the gas becomes visible, the earlier it scrambles. Figure 9 shows that a high injection rate warrants a low PV to reach the gas-visibility state; that is, the gas-visibility time is shortened, and the ripple coefficient first increases rapidly and then moderately slowly with the increasing injection rate. A small increment in the gas injection rate increases the speed of propulsion, thus increasing the wave coefficient and shortening the gas-visibility time. However, under this condition, the diffusion coefficient of carbon dioxide remains unchanged, and a substantially high speed results in a decrease in the amount of carbon dioxide dissolved in the crude-oil gas, thus decreasing the wave coefficient. An extremely high injection rate results in the early emergence of gas channeling, and an emission of more than 1600 m^3/t of gas shuts down the well. When the injection rate is 1.25 × 10^4 $m^3·d^{-1}$, the gas flurry emerges at a delayed time and a large wave coefficient is obtained; these features are consistent with the requirements for regulating gas channeling.

Figure 10 shows that the higher the gas-to-water ratio, the shorter the time to see the gas and the more serious the gas channeling phenomenon. Figure 11 indicates that at the gas−

https://doi.org/10.1021/acsomega.3c09718
ACS Omega 2024, 9, 9655−9665

Table 4. Summary of the Results of Different Experimental Protocols

	factors				evaluation indices			
scheme number	gas injection rate ($\times 10^4$ $m^3 \cdot d^{-1}$)	gas injection period (mon)	gas−water ratio ($m^3 \cdot m^{-3}$)	bottom-hole flowing pressure (MPa)	recovery efficiency (%)	oil exchange ratio (%)	formation pressure (MPa)	CO_2 storage rate (%)
1	1.0	2	1:1	10	17.49	20.13	24.9	45.7
2	1.0	3	1:2	15	20.36	23.1	22.9	48.8
3	1.0	4	2:1	20	12.88	19.88	24.4	39.6
4	1.0	5	1:3	25	12.08	24.11	25.6	43.2
5	1.25	2	1:2	20	20.21	19.1	27	52.1
6	1.25	3	1:1	25	20.74	21.33	27.8	49.4
7	1.25	4	1:3	10	13.04	19.73	26.9	50.9
8	1.25	5	2:1	15	12.22	23.57	25	56.7
9	1.50	2	2:1	25	20.24	24.6	23	58
10	1.50	3	1:3	20	20.69	21.37	22.1	57.9
11	1.50	4	1:1	15	13.15	17.8	24.9	52.1
12	1.50	5	1:2	10	12.2	23.43	21	53.4
13	1.75	2	1:3	15	20.24	20.3	22.9	49.1
14	1.75	3	2:1	10	21.01	19.86	24.8	44.2
15	1.75	4	1:2	25	13.57	25.2	25.7	45.6
16	1.75	5	1:1	20	12.42	23.11	26.7	45.7

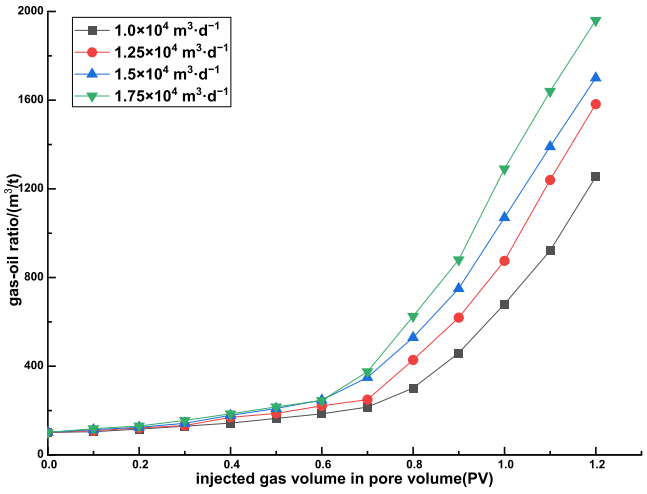

Figure 8. Variations in the gas-oil ratio at different injection rates.

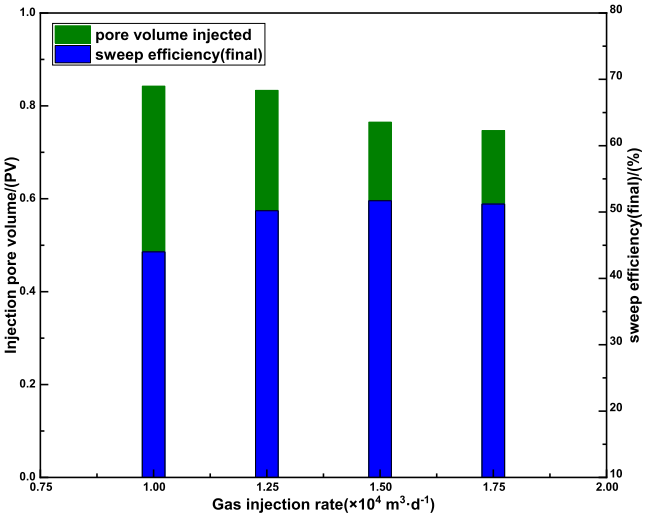

Figure 9. Gas breakthrough time and sweep efficiency at different gas injection rates.

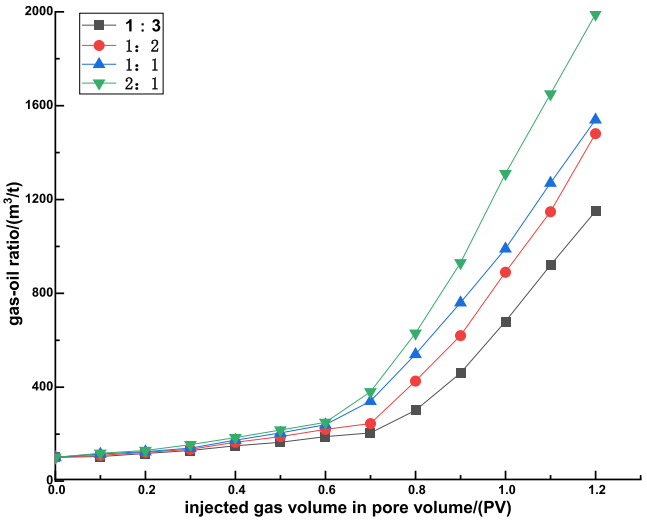

Figure 10. Variation curves of gas−oil ratio at different gas−water ratios.

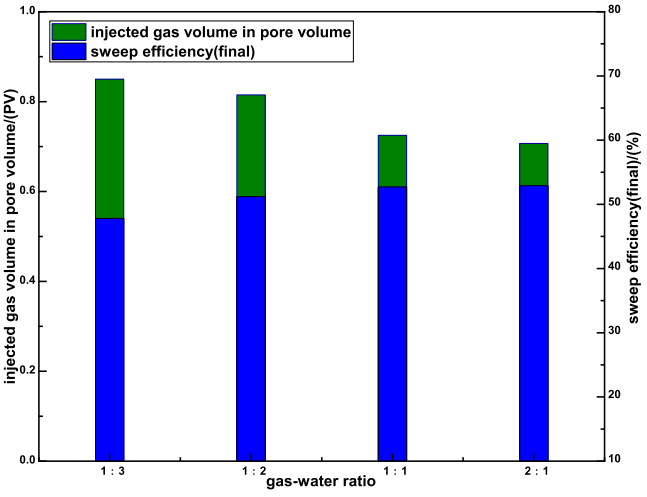

Figure 11. Gas breakthrough time and sweep efficiency at different gas-to-water ratios.

https://doi.org/10.1021/acsomega.3c09718
ACS Omega 2024, 9, 9655−9665

water ratios of 1:3 and 1:2, the gas starts appearing when the gas with a volume ∼0.8 times the PV is injected. At gas-to-water ratios of 1:1 or 2:1, the gas starts appearing when the gas with a volume ∼0.7 times the PV is injected. Further, the higher the gas-to-water ratio, the larger the wave coefficient of carbon dioxide at the time of gas visibility, the earlier the gas becomes visible, and the earlier gas scrambling occurs. Thus, a gas−water ratio of 1:1 ensures safe production to a certain extent; in this case, the wave coefficient is also sufficiently high and meets the requirements for prevention and control of CO_2 flooding gas channeling.

4. RESULTS AND DISCUSSION

4.1. Comparison of Formation Pressure before and after Carbon Dioxide Injection. The well group 80513 was used as the test injection well set with 0.018 times the PV occupied by hydrocarbons of CO_2 injected on-site during the preinjection period. Figure 12 shows the formation pressure data of seven wells in this well group measured during the test period. Evidently, the formation pressure increases after gas injection, and the formation pressure of well 80513 for 60 days of test injection is ∼8 MPa higher than that before the test injection. As the injection volume increases during the test injection process, the formation pressure around the wellbore rapidly increases and fluctuates between 22 and 45 MPa; at this time, energy accumulation occurs primarily at the bottom of the well, and this accumulated energy does not reach the boundary. In the mining phase, energy is constantly consumed as the mining proceeds, and eventually, it slowly ripples toward the boundary with a noticeable pressure drop.

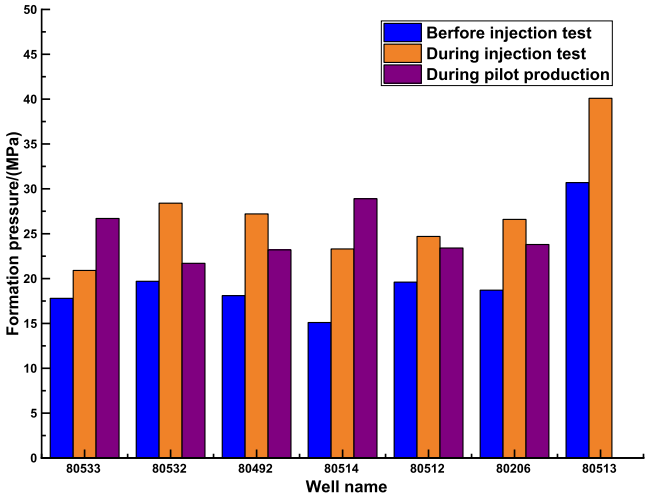

Figure 12. Changes in formation pressure before and after the injection test of the target well group.

The established numerical simulation model is used to calculate the changes in the formation pressure after 60 days of gas injection. Figure 13 reveals that the formation pressure in the block, in which the target well group is located, increases after the CO_2 flooding, and energy restoration is realized.

4.2. Comparison of Oil Production before and after CO_2 Injection. Next, we compare the monthly oil production from two well packages, 80534 (water-driven) and 80513 (gas-driven), with similar well conditions in the field. Results of the comparison of the monthly oil production from January 2011 to June 2018 for the water-driven well group and the 80513 well group are depicted in Figure 14. Evidently, the average monthly oil production of both the well groups (80534 and 80513) was around 110 t in 2016−2017 when they were in the water-driven phase. Upon carbon dioxide injection in the well group 80513, the average monthly oil production from December 2017 to June 2018 reached 201.4 t, which is 1.85 times higher than that observed in the preinjection period. The field data indicate that after six months of CO_2 test injection in the well group 80513, a total of 2035 t of crude oil is extracted during the test recovery phase. The oil exchange rate for a water-driven injection volume of 14,334 m^3 significantly increases; in this case, only 120 t of cumulative oil production is detected. In contrast, when the gas-driven well group's injection volume is 3789.8 m^3, the cumulative oil production is 10 times more than that of the water-driven stage. After carbon dioxide injection, block phase extraction drastically improves.

Carbon dioxide flooding began in the 80513 well group in December 2017, with a historical fitted time frame of December 2017 to January 2023. The predicted results indicate that the amount of carbon dioxide that can be extracted from well group 80513 in block K via carbon dioxide flooding will require 15 injection and 43 extraction events. Further, approximately 1.92 million tons of geological reserves will be utilized to form a scale of 100,000 tons of carbon dioxide injection per year. The rate of recovery is expected to be > 25 75% for a 15 year test cycle.

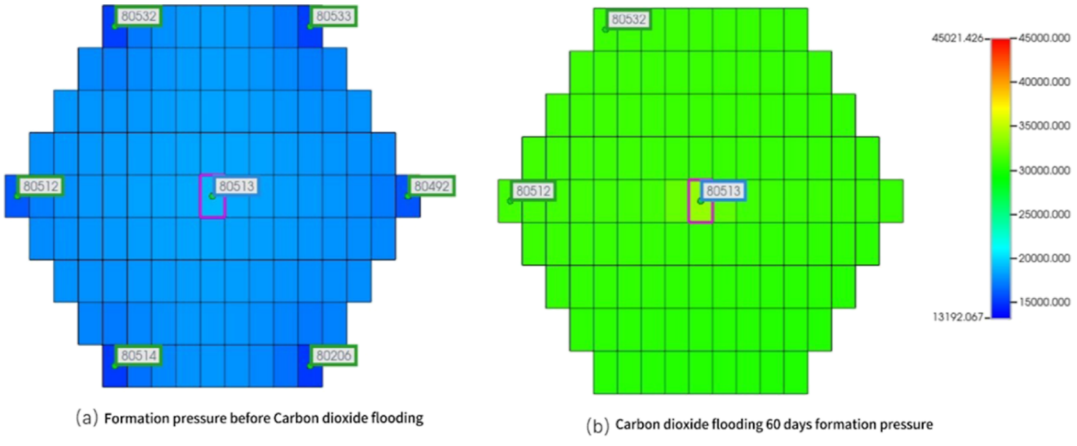

Figure 13. Changes in formation pressure before and after carbon dioxide injection in well group 80513.

https://doi.org/10.1021/acsomega.3c09718
ACS Omega 2024, 9, 9655−9665

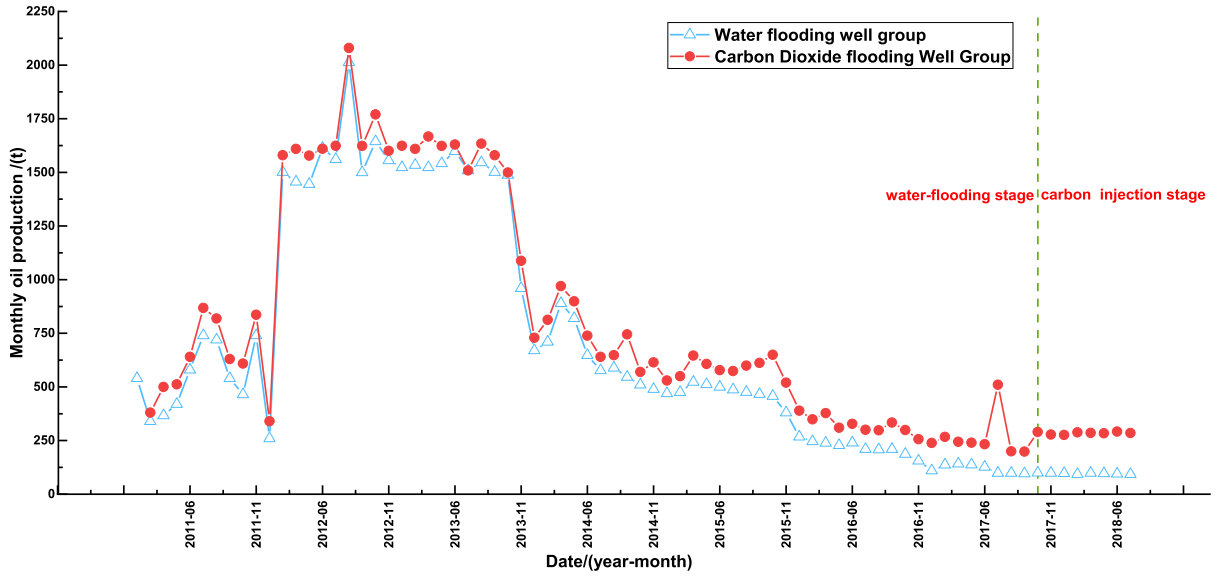

Figure 14. Comparison between the oil production of the water drive and CO_2-flooding well groups.

5. CONCLUSIONS

(1) Combined with the flow and material characteristics of the target block, the CO_2-flooding numerical simulation model based on the 80513 well group demonstrated the specific development plan of the zone and provided a complete idea of injection. The established numerical model of water-sensitive post-CO_2 flooding is well aligned with the field development conditions, and the optimized parameters can be easily implemented. Previous studies indicate that this parameter optimization considers the important economic indicators in the mining process as well as evaluates the feasibility of regulating CO_2 flooding gas channeling, thus providing comprehensive optimization results. Overall, the simulation study carried out for the well group 80513 will boost CO_2 flooding and recovery enhancement in block K.

(2) In view of the development of the target block, the time of development was designed as follows: energy recovery, continuous gas injection, and regulation and optimization phases. In the previous numerical simulation of injection parameters, the indicators for optimization and selection were combined, and the simulation model, parameter optimization, and research and judgment of the indicators were different for different stages of the separate optimization design. These models and optimization processes, especially the optimization stage of the control, were based on the orthogonal design theory and accordingly considered enhanced recovery and prevention of gas flurry. They also compared different injection rates, gas−water ratios, gas times, and other such parameters to assess the influence of the parameter optimization results on controlling gas flurry. Thus, a targeted and comprehensive simulation of the wells was performed to rationally design the injection scheme.

(3) Field application showed that the oil recovery efficiency of the 80513 well group improves after CO_2 flooding extraction. Moreover, field data and the model simulation results showed that CO_2 flooding increased the formation pressure and oil recovery efficiency in this block. A comparison between the formation pressures before and after carbon dioxide injection revealed that the carbon dioxide flooding supplemented the formation energy. The average monthly oil production of the 80513 well group reached 201.4 t in the first half year after the trial carbon dioxide injection; this value is 1.85 times that observed before the gas injection. Based on the mining situation of the well group 80513, we can predict that if CO_2 flooding is carried out in the K-zone Keshita group, then a scale of 15 injection and 43 extraction can be formed, and it is expected that 1.92 million tons of geological reserves will be utilized. Further, based on the calculation of a 15-year test cycle, we expect that the recovery rate will be more than 25.75%.

AUTHOR INFORMATION

Corresponding Author

Meilong Fu − *Hubei Provincial Key Laboratory of Oil and Gas Drilling and Production Engineering, School of Petroleum Engineering, Yangtze University, Wuhan 430100, China*; Email: fmlytze@163.com

Authors

Xu Deng − *Hubei Provincial Key Laboratory of Oil and Gas Drilling and Production Engineering, School of Petroleum Engineering, Yangtze University, Wuhan 430100, China*; orcid.org/0009-0004-0284-0000

Jie Li − *Shaanxi Yanchang Petroleum Fengyuan Co., Ltd., Yan'an 716000, China*

Jiani Hu − *Hubei Provincial Key Laboratory of Oil and Gas Drilling and Production Engineering, School of Petroleum Engineering, Yangtze University, Wuhan 430100, China*

Guojun Li − *Hubei Provincial Key Laboratory of Oil and Gas Drilling and Production Engineering, School of Petroleum Engineering, Yangtze University, Wuhan 430100, China*

Fankun Meng − *Hubei Provincial Key Laboratory of Oil and Gas Drilling and Production Engineering, School of Petroleum Engineering, Yangtze University, Wuhan 430100, China*

https://doi.org/10.1021/acsomega.3c09718
ACS Omega 2024, 9, 9655−9665

Complete contact information is available at:
https://pubs.acs.org/10.1021/acsomega.3c09718

Notes

The authors declare no competing financial interest.

■ ACKNOWLEDGMENTS

Our study "Research on characterization, identification, and optimization of CO_2 gas flow channels in low-permeability reservoirs" (no. 52104018) was financially supported by the National Natural Science Foundation of China, for which we are grateful. We are appreciative to T Oilfield for supplying the geological information and physical parameters needed for the numerical simulation model. We are appreciative of Yangtze University for supplying the lab space and other necessary equipment.

■ REFERENCES

(1) Li, J. Z.; Zheng, M.; Chen, X. M.; et al. Identification of unconventional oil and gas connotation, source−reservoir combination types and unconventional oil and gas development potential in China. *Acta Petrol. Sin.* **2015**, *36* (05), 521−532.
(2) Zhou, C. N.; Tao, S. Z.; Bai, B.; et al. On the difference and connection between unconventional and conventional oil and gas. *China Pet. Explor.* **2015**, *20* (01), 1−16.
(3) Niu, S. W. Exploration and practice of geological engineering integration in low-permeability tight reservoirs of Shengli oilfield. *China Pet. Explor.* **2023**, *28* (01), 14−25.
(4) Zhou, C. N.; Wu, S. T.; Yang, Z.; et al. Progress, challenge and significance of building a carbon industry system in the context of carbon neutrality strategy. *Pet. Explor. Dev.* **2023**, *50* (01), 190−205.
(5) Zhang, X.; Li, Y.; Ma, Q.; Liu, L. Development of Carbon Capture, Utilization and Storage Technology in China. *Strateg. Stud. CAE* **2021**, *23* (6), 70−80.
(6) Li, Y.; Zhao, Q. M.; Xue, Z. j. *Oil Drilling and Production Technology*; Oriprobe, 2023, pp 1−9.CCUS technological and industrialization development path under the target ofcarbon peaking and carbon neutrality
(7) Li, G. C. Progress of main enhanced oil recovery technologies for oilfields in China(II). *Oilfield Chem.* **2023**, *40* (1), 175−181.
(8) Tang, Y.; Liu, M. Y.; Qin, J. Z.; et al. A evaluation method of CO_2 sequestration potential in gas reservoirs based on mole balance. *Oil Drill. Prod. Technol.* **2023**, *45* (2), 197−202.
(9) Liao, G.; He, D.; Wang, G.; Wang, L.; Wang, Z.; Su, C.; Qin, Q.; Bai, J.; Hu, Z.; Huang, Z.; et al. Discussion on the limit recovery factor of carbon dioxide flooding in a permanent sequestration scenario. *Pet. Explor. Dev.* **2022**, *49* (6), 1463−1470.
(10) Cui, C. Z.; Su, X. K.; Y, T. Y.; et al. Sweep characteristics of CO_2 miscible flooding with injection-recovery coupling in low-permeability reservoirs and quantitative classification of gas channeling stages. *Spec. Oil Gas Reservoirs* **2022**, *29* (4), 90−95.
(11) Yang, D.; Gu, Y. Determination of diffusion coefficients and interface mass-transfer coefficients of the crude oil CO_2 system byanalysis of the dynamic and equilibrium interfacial tensions. *Ind. Eng. Chem. Res.* **2008**, *47* (15), 5447−5455.
(12) Liu, J. Y.; Yang, X.; Liu, Y. Phase state and component change law of CO_2 flooding in low-permeability sandstone reservoirs. *Spec. Oil Gas Reservoirs* **2022**, *29* (6), 91−96.
(13) Qi, C. M.; Li, R. D.; Zhu, S. D.; et al. Pilot test of carbon dioxide flooding in low-permeability reservoirs in the long $4 + 5^1$ area of Yun gou district, Ordos basin. *Oil Drill. Prod. Technol.* **2019**, *41* (2), 249−253.
(14) Cheng, J. C.; Jiang, H. F.; Lei, Y. Z.; et al. Study on miscible CO_2 flooding test in strong water-sensitive reservoirs in sudert oilfield. *Xinjiang Pet. Geol.* **2016**, *37* (6), 694−696.
(15) Zhao, N.; Wang, L.; S, L.; et al. Indoor evaluation of gas injection development in low-permeability reservoirs under different injection gases. *Sci. Technol. Eng.* **2020**, *20* (4), 1379−1385.
(16) Qin, J. H.; Han, H. S.; Liu, X. L. Application and enlightenment of carbon dioxide flooding in the United States of America. *Pet. Explor. Dev.* **2015**, *42* (2), 209−216.
(17) Li, S. L.; Sun, L.; Chen, Z. H.; et al. Further discussion on reservoir engineering concept and development mode of CO_2 flooding-EOR technology. *Reservoirs* **2020**, *10* (30), 1−14.
(18) Xia, W. M.; Wang, X. M.; Lei, J. Q. The optimization of well patterns of CO_2-flooding for low-permeable reservoir. *Lithol. Reservoirs* **2009**, *21* (4), 105−107.
(19) Song, Z. J.; Li, Z. P.; Lai, F. P.; et al. Optimization and evaluation of CO_2 flooding parameters for water flooding reservoir conversion. *J. Xi'an Shiyou Univ.* **2012**, *27* (6), 42−47.
(20) Shang, B. B.; Liao, X. W.; Lu, N.; et al. Optimization of alternate water and gas injection parameters for CO_2 flooding-an example of long 6 reservoir in Wang Yao block of Ansai oilfield. *Pet. Geol. Recovery Effic.* **2014**, *21* (3), 70−72.
(21) Wang, H.; Ji, B. Y.; Zhao, S. X.; et al. Study on feasibility of CO_2 flooding and storage in complex fault-block tight reservoir. *J. Shaanxi Univ. Sci. Technol.* **2022**, *40* (3), 115−122.
(22) Bai, J. Feasibility Study of CO_2 flooding in very low permeability strongly water-sensitive reservoir. *Sci. Technol. Eng.* **2012**, *12* (21), 5270−5273.
(23) Lu, T.; Li, Z. M.; Liu, W.; et al. Research on CO_2 throughput technology for strongly water-sensitive thickoil reservoirs. *J. Xi'an Shiyou Univ.* **2013**, *35* (1), 122−128.
(24) Zhuang, Y. T.; Liu, P. C.; Zhang, J. Y.; et al. Optimization study of CO_2 injection and recovery parameters in outer Daqing oilfield. *Drill. Prod. Technol.* **2014**, *37* (1), 42−46.
(25) Zhao, L. X.; Zhang, Z. C.; Zhu, A. J. Research on antiexpansion water injection technology under 530 grams in eight districtsXinjiang. *Oil Gas* **2014**, *10* (01), 78−82.
(26) Soave, G. Equilibrium constants from a modified Redlich-Kwong equation of state. *Chem. Eng. Sci.* **1972**, *27* (6), 1197−1203.
(27) Peng, D. Y.; Robinson, D. B. A New Two-Constant Equation of State. *Ind. Eng. Chem. Res. Fundamentals* **1976**, *15* (1), 59−64.
(28) Kwak, T. Y.; Mansoori, G.; Mansoori, G. A. Van der waals mixing rules for cubic equations of state. Applications for supercritical fluid extraction modelling. *Chem. Eng. Sci.* **1986**, *41* (5), 1303−1309.
(29) Gao, B.; Xu, S. J.; Hu, X. L.; et al. Experimental study on the influence of water sensitivity on oil-water two-phase seepage in low permeability reservoirs. *J. Xi'an Shiyou Univ.* **2022**, *37* (06), 75−81.
(30) Yu, J. B. A method for calculating the history fitting accuracy of numerical simulations of reservoirs Xinjiang. *Pet. Geol.* **2015**, *36* (03), 304−307.
(31) Ma, Q. Z.; Yang, S. L.; Wang, M. B.; et al. Experimental investigation on minimum miscible pressure of the tight oil reservoir in Jimsar Sag, Xinjiang. *J. Liaoning Shihua Univ.* **2020**, *40* (1), 35−38.
(32) Yang, B.; Tang, R. Z.; Luan, C. Z.; et al. The technology of preventing CO_2 breakthrough and gravity segregation abroad. *Fault-Block Oil Gas Field* **2003**, *3* (2), 64−66.
(33) Zhao, Q. M.; Lun, Z. M.; Zhao, S. X. Characterization of CO_2 flooding in low permeability inhomogeneous reservoirs and hydrodynamic tamponade sealing methods. *Pet. Reservoir Evaluation Dev.* **2019**, *9* (03), 62−65.
(34) Bai, S.; Song, K. P.; Yang, E. L.; et al. Simulation of orthogonal experimental design of CO_2 flooding water and gas alternating injection parameters. *Spec.oirs* **2011**, *18* (01), 105−108.
(35) Li, N.; Pan, Z. J.; S, T.; et al. Design of orthogonal experiments and optimization of numerical simulation for CO_2 flooding in ultralow-permeability reservoirs. *Xinjiang Pet. Geol.* **2017**, *38* (01), 62−65.
(36) Yu, P.; Yang, F. L.; Kegang, L.; et al. Optimization of carbon dioxide utilization and storage parameters based on multi-indicator orthogonal schematic design. *Math. Pract. Theory* **2020**, *50* (15), 96−103.

(37) Zhang, M.; Zhao, F. L.; Lu, G. Z.; et al. Adaptation boundaries of gas−water alternation to improve carbon dioxideoil repelling effect. *Oilfield Chem.* **2020**, *37* (2), 279−286.

https://doi.org/10.1021/acsomega.3c09718
ACS Omega 2024, 9, 9655−9665